Silica-magnesium-titanium Ziegler–Natta catalysts. Part II. Properties of the active sites and fragmentation behaviour

Journal of Catalysis 423 (2023) 10–18

Contents lists available at ScienceDirect

Journal of Catalysis

journal homepage: www.elsevier.com/locate/jcat

Silica-magnesium-titanium Ziegler–Natta catalysts. Part II. Properties of the active sites and fragmentation behaviour

Jelena Zarupski [a,b], Alessandro Piovano [a,b,1], Maximilian J. Werny [b,c], Andrea Martini [a,2], Luca Braglia [d], Piero Torelli [d], Coen Hendriksen [b,e], Nicolaas H. Friederichs [b,e], Florian Meirer [b,c], Bert M. Weckhuysen [b,c], Elena Groppo [a,b,*]

[a] Department of Chemistry, INSTM and NIS Centre, University of Torino, Via Giuria 7, 10125 Torino, Italy
[b] Dutch Polymer Institute, P.O. Box 902, 5600 AX Eindhoven, The Netherland
[c] Inorganic Chemistry and Catalysis Group, Institute for Sustainable and Circular Chemistry and Debye Institute for Nanomaterials Science, Utrecht University, 3584 CG Utrecht, The Netherlands
[d] CNR-IOM, TASC Laboratory, 34149 Trieste, Italy
[e] SABIC Technology Center, 6167 RD Geleen, The Netherlands

ARTICLE INFO

Article history:
Received 6 February 2023
Revised 21 April 2023
Accepted 24 April 2023
Available online 29 April 2023

Keywords:
Ziegler–Natta catalysts
Spectroscopic methods
Ti-alkyl
Olefin polymerization kinetics
Particle fragmentation

ABSTRACT

In this work, which follows Part I that is dedicated to the precatalyst, we investigate the electronic properties and the accessibility of the Ti active sites in a highly active silica-supported Ziegler–Natta catalyst for industrial polyethylene production, applying a multi-scale, multi-technique approach. Complementary electronic spectroscopies (i.e. Ti K-edge XANES, Ti $L_{2,3}$-edge NEXAFS and DR UV–Vis-NIR) reveal the coexistence of several titanium phases, whose relative amount depends on the concentration of the alkyl aluminum activator. In addition to β-$TiCl_3$-like clusters and monomeric Ti(IV) sites, which are already present in the precatalyst, isolated Ti(III) sites and α-$TiCl_3$-like clusters are formed in the presence of the activator. Two families of alkylated Ti(III) sites characterized by a different electron density are detected by IR spectroscopy of adsorbed CO, and two types of Ti-acyl species are formed upon CO insertion into the Ti-alkyl bond, characterized by a different extent of η^2-coordination. The whole set of data suggests that $TiCl_3$ clusters are preferentially formed at the exterior of the catalyst particles, likely as a consequence of Ti(III) mobility in the presence of strong Lewis acids, in most cases hampering the spectroscopic detection of isolated Ti(III) sites. In contrast, only monomeric Ti(III) sites are formed at the interior of the catalyst particles, characterized by a high electron density evocative of the presence of electron donors in the close proximity (e.g. aluminum alkoxide by-products). These sites are less accessible because of diffusion limitations, and only become visible by surface-sensitive spectroscopic methods (such as Ti $L_{2,3}$-edge TEY-NEXAFS) upon the fragmentation of the catalyst particles.

1. Introduction

Silica-supported Ziegler–Natta (ZN) catalyst materials play a major role in the industrial manufacture of polyethylene (PE) and polypropylene (PP). The amorphous silicas commonly adopted as supports display high specific surface areas as a consequence of intraparticle porosity and exposed hydroxyl groups and/or strained siloxane bridges at the surface, which are potentially reactive [1]. Both factors may influence the catalyst synthesis as well as their behaviour in olefin (co)-polymerization [2], and explain why silica-supported ZN catalyst materials are unsurpassed in the slurry-phase and gas-phase ethylene polymerization processes, where the particle size of the final PE granule is fundamental for maintaining excellent reactor continuity. In particular, the chemical properties (e.g., relative amount of silanol groups and siloxane bridges) determine the structure of the active sites at a molecular level, while the physical properties (e.g., porosity, specific surface area, and pore space connectivity) govern phenomena, like the diffusion of the monomer into the pores, the steric accessibility, and the particle fragmentation [3,4]. This latter phenomenon is particularly relevant in olefin polymerization catalysis, because it is essential for assuring high activity and for controlling polymer

* Corresponding author.
E-mail address: elena.groppo@unito.it (E. Groppo).
[1] Current address: GAME Lab, Department of Applied Science and Technology, Polytechnic of Torino, Corso Duca Degli Abruzzi, 24, 10129 Torino, Italy.
[2] Current address: Department of Interface Science, Fritz- Haber Institute of the Max-Planck Society, 14195 Berlin, Germany.

https://doi.org/10.1016/j.jcat.2023.04.015
0021-9517/

morphology. Catalyst particle fragmentation occurs when a sufficient amount of solid polymer is formed at the active sites, building up mechanical forces that cause the disintegration into submicron primary particles dispersed throughout the polymer granule. This is fundamental to avoid mass transfer limitations and pore blocking by the solid polymer as well as to continuously expose active sites to the incoming monomer.

There exist a large variety of methods for producing silica-supported ZN catalysts, and many of them have been excellently reviewed by Pullukat [2]. In most cases, the synthesis procedure involves multiple components mixed in solution (e.g., a magnesium compound, a titanium compound, and an organic electron donor), which are either grafted at the silica surface through surface reactive groups, or simultaneously precipitated at the silica surface in the form of self-standing catalyst complexes (in the latter case, silica should be formerly highly dehydroxylated by chemical means). The final result is very much dependent on the synthesis parameters. The patent literature contains a lot of information on how small changes in the synthesis procedure may lead to great changes in the properties of the polymer produced, in terms of e.g., molecular weight distribution (MWD) and comonomer incorporation [5–7]. However, in most cases the molecular structure of the catalyst is not known and only a few hypotheses are made based on chemical intuition. This may explain why silica-based ZN catalysts still attract a lot of scientific interest in addition to their commercial importance.

The present paper focuses on a particular type of silica-supported ZN catalyst, obtained by reacting together a chemically dehydroxylated silica with a solution of an organomagnesium compounds and $TiCl_4$ in the presence of 1-butanol as modifier [5]. In Part 1 of this work [8], by synergistically coupling a series of advanced physicochemical methods, we have been able to disclose the molecular structure of the precatalyst. In particular, we found that two Ti phases co-exist: a Ti(III) phase with electronic properties similar to those of the β-$TiCl_3$ polymorph, but highly dispersed, and monomeric 6-fold coordinated Ti(IV) sites, mostly surrounded by chlorine ligands, but possibly also by some butoxide moieties. The monomeric Ti(IV) sites have a structure similar to that of Ti(IV) sites in $TiCl_4$-capped $MgCl_2$ nanoplates, as predicted by combining a genetic algorithm with density functional theory (DFT) calculations [9], with three different Ti-Cl distances. Moreover, the Ti(IV) sites are intimately interconnected with nanosized $MgCl_2$. Hence, we have proposed the presence of mixed oxochloride magnesium-titanium structures in the precatalyst material, having an almost molecular character. While the local structure of the precatalyst surely affects the behaviour of the catalyst material in olefin polymerization conditions, it is also well known that the aluminium-alkyl activator may partially reconstruct the catalytically active phase, not only in terms of titanium sites but also considering the $MgCl_2$ phase as well. This was demonstrated by some of us for a silica-supported ZN catalyst obtained by reacting together titanium and magnesium chloride tetrahydrofuranate precursors, both in the absence [10,11] and in the presence of dehydroxylated silica [12,13].

Herein we deepen the investigation of our silica-magnesium-titanium system, by studying the effect of the aluminium-alkyl activator on the molecular structure of the catalyst. In particular we focus our attention on the structural and electronic properties of the Ti sites in the activated catalyst as a function of both the concentration and the type of the activator. Moreover, we study the accessibility of the activated Ti sites to carbon monoxide, which was selected as insertion probe to mimic the interaction of the catalyst with the monomer, because it is known that CO can insert into metal-alkyl bonds, exactly as the monomer does during the polymerization [14]. This reactivity has been long exploited in industry not only to temporarily quenching the reaction rate when it proceeds too fast, thus avoiding reactor fouling, but also for counting the sites active in olefin polymerization, using the so called "tagging approach" [15–21]. Finally, we investigate the behaviour of the catalyst in action by studying the kinetics of gas phase ethylene polymerization in very mild conditions (comparable to those used for the spectroscopic measurements) and the catalyst fragmentation behaviour in slurry conditions. The whole set of data offer an unprecedent view on the spatial distribution of the different Ti phases in the catalyst particles.

2. Experimental

2.1. Precatalyst activation by aluminium compounds

The ZN precatalyst material was provided by SABIC and synthetized according to the procedure described in patent by Pullukat and Hoff [5], and summarized in Part 1 of this work [8]. The precatalyst was activated prior each measurement according to the following procedure: inside the glovebox a weighted amount of powder was first impregnated with anhydrous hexane (to completely fill the pores), and then with diluted aluminium alkyl, attaining the desired Al/Ti stoichiometry. This procedure was optimized in order to slow down the interaction of the activator with the Ti phase. In fact, a dry impregnation procedure would imply a rapid filling of the pores by the activator, which generates an undesired gradient of concentration in the catalyst particles. Even though it is not uncommon in industry to use tri-isobutylaluminium (TIBA) at Al/Ti molar ratios of for instance 3.25, we performed most of the experiments with triethylaluminium (TEAl) using n-hexane as a solvent to simplify subsequent spectroscopic measurements. We also explored the effect of different amounts of activator in the range 1/1 to 10/1. Some measurements were replicated with tri-isobutylaluminium (TIBA) (1 M in hexanes). After preparation the wet powder was transferred inside the measuring cell. The remaining solvent was gently removed by degassing in high vacuum or by flowing the cell with He (for NEXAFS measurements). For Fourier transform infrared (FT-IR) spectroscopy measurements, the activated powder was partially dried inside the glovebox, pressed in form of a pellet and then transferred inside the measuring cell. The remaining solvent was removed by degassing in high vacuum.

2.2. Characterization methods

2.2.1. Ti K-edge X-ray absorption spectroscopy

Ti K-edge X-ray absorption spectroscopy (XAS) measurements in transmission mode were performed at the XAFS beamline at the Elettra Sincrotrone Trieste facility. The catalyst, activated with different amounts of TEAl in the glovebox was diluted in dehydrated boron nitride (BN) and pressed in the form of a pellet, sealed inside a low-density polyethylene (LDPE) envelope under vacuum, and finally transferred in the measurement chamber at the beamline without exposure to air. Details on the settings of the beamline, data acquisition and related data processing have been reported in Part 1 of this work [8].

2.2.2. Ti $L_{2,3}$-edge NEXAFS spectroscopy

Ti $L_{2,3}$-edge Near-Edge X-ray Absorption Fine Structure (NEXAFS) spectra were collected at the APE-HE beamline of the Elettra Sincrotrone Trieste facility, in the total electron yield (TEY) mode. The catalyst, activated inside the glovebox with TEAl at a ratio Al/Ti = 3.25, was pressed inside a thin indium plate (to ensure the electrical conductivity), and placed inside an ambient-pressure NEXAFS cell, avoiding any contact with air [22]. All measurements were performed under a 5 mL min^{-1} He flow at 1 bar.

For investigating ethylene polymerization, small ethylene pulses were added to the He flow, as already described in our previous work [23]. Further details about the settings of the beamline, data acquisition and related data processing have been reported in Part 1 of this work [8].

2.2.3. Diffuse reflectance UV–Vis-NIR spectroscopy

UV – Vis-NIR spectra were collected in the diffuse reflectance (DR) mode with a Varian Cary5000 spectrophotometer. The catalyst powder, activated with TEAl in different amounts in the glovebox, was first dried under vacuum and then transferred in a custom-made bulb cell in optical quartz (suprasil) without further exposure to air. The spectra were collected in reflectance mode (R %) and subsequently converted applying the Kubelka–Munk F(R) function.

2.2.4. Ft-Ir spectroscopy of adsorbed CO

A series of transmission Fourier-transform infrared (FT-IR) experiments in the presence of CO as molecular probe were performed on the catalyst activated with 3.25 eq. of TEAl. All the spectra were collected at a resolution of 2 cm^{-1} by means of a Bruker Vertex 70 spectrophotometer equipped with a MCT detector. The activated catalyst was pressed in the form of a thin self-supporting pellet inside the glovebox and inserted into a home-made cell to perform measurements in the presence of a controlled pressure of gases at a controlled temperature. CO adsorption at 100 K was performed as described in Part 1 of this work [8]. The experiments at room temperature, instead, were performed as follows: after measuring the spectrum of the activated catalyst at room temperature, CO was admitted in the cell at an equilibrium pressure P_{CO} = 50 mbar, and the FT-IR spectra were continuously collected every 3 min for 1 h at constant temperature. After that, CO was removed from the cell. In another type of experiment (reported in the Supporting Information), CO was dosed on a catalyst after a short pre-polymerization step under very mild conditions (ethylene pressure = 50 mbar, room temperature, 10 min).

2.3. Kinetics of gas-phase ethylene polymerization under mild conditions

The kinetic of gas-phase ethylene polymerization was monitored under mild conditions as follows: Approximately 100 mg of the precatalyst were activated in the glovebox with the desired amount of TEAl, following the procedure described in Section 2.1. The wet powder was transferred into a quartz tube cell in the glovebox, and then connected to a vacuum line for faster drying. Ethylene was then admitted into the tube cell, and ethylene pressure was continuously monitored as a function of time for 15 min.

2.4. Focused ion beam-scanning electron microscopy on pre-polymerized catalyst particles

Ethylene pre-polymerization was performed at room temperature in slurry-phase at 1.0 bar ethylene pressure. The desired amount of co-catalyst (either TEAl or TiBA) and 10 mL heptane were added to a glass reactor loaded with 10 mg catalyst inside the glovebox. After briefly evacuating the reactor (~2 s) to remove the nitrogen atmosphere, the reactor was pressurized with ethylene for 1 min under stirring (i.e., 600 rpm). A brief vacuum was then applied to remove the ethylene, the stirring turned off and the reactor opened. Following this, the heptane was decanted, and the polymer dried under air flow outside of the glovebox. The polymer was weighed to determine the catalysts' respective productivities (i.e., polyethylene yields).

A FEI Helios NanoLab G3 UC scanning electron microscope (SEM) was used to study the external and internal morphology of selected catalyst samples following procedures from literature [24,25]. The pre-polymerized samples were dispersed onto a double-sided adhesive, conductive carbon tape on an aluminium SEM stub. Prior to the FIB-SEM measurements, a Pt coating of ~6 nm thickness was applied with a Cressington 208HR sputter coater to improve the conductivity of the sample. All particles were cut parallel to the surface of the stub using a 45° angled SEM stub at different stage tilt angles. The cross-sectional images were acquired in backscattered electron (BSE) mode at 2 kV and 0.1 nA using a Through the Lens Detector (TLD) and an immersion lens.

3. Results and discussion

3.1. Electronic properties: A two-step reduction as a function of the Al/Ti ratio

As a first step, we have investigated the electronic properties of the Ti sites in the catalyst activated with different amounts of TEAl. Fig. 1 shows the Ti K-edge XAS, the Ti $L_{2,3}$-edge NEXAFS and the DR UV–Vis-NIR spectra of the precatalyst and of some of the activated catalyst materials. In Part 1 of this work [8], we have already demonstrated the potential of this combined approach. Starting the discussion from the Ti K-edge XANES spectra (Fig. 1A), the most relevant changes observed upon addition of TEAl to the precatalyst are: 1) a gradual shift of the edge towards lower energy of about 0.7 eV for Al/Ti = 1.0, 1.0 eV for Al/Ti = 3.25, and up to about 2.0 eV for Al/Ti = 10.0; 2) an attenuation in the intensity and a shift in energy of the pre-edge peak (inset in Fig. 1A). Up to 3.25 eq. of TEAl, the changes observed in the XANES spectra indicate that a fraction of the Ti(IV) in the precatalyst are reduced to Ti(III) species. Through a linear combination of the two reference spectra we obtain that at Al/Ti = 1.0 roughly 58(±2)% of the Ti is Ti(III), while at Al/Ti = 3.25 the fraction increases up to approximately 67(±2)%. At the highest Al/Ti ratio, instead, over-reduction of a fraction of the Ti sites to Ti(II) species occurs [26]. This process likely involved the $TiCl_3$ clusters already present in the precatalyst (*vide infra*, EXAFS data).

$L_{2,3}$-edge NEXAFS spectroscopy (Fig. 1B) seems less sensible to the activation procedure than Ti K-edge XANES spectroscopy. In fact, the $L_{2,3}$-edge NEXAFS spectrum of the catalyst activated with 3.25 eq. of TEAl is still similar to that of the precatalyst. The most relevant change is the decrease in intensity of the peak at 458.3 eV, attributed to the electronic transition from the Ti $2p_{3/2}$ orbitals to the Ti d_{t2g} orbitals. This is indicative of the reduction of a fraction of Ti(IV) to Ti(III) sites, since for Ti(III) the d_{t2g} orbitals are already occupied by one electron, while for Ti(IV) they are totally empty, hence resulting in a lower probability for this electronic transition compared to Ti(IV). Nevertheless, the changes in the spectrum upon catalyst activation are much less than expected for the reduction of a substantial fraction of Ti(IV) to Ti(III), as determined by XANES. We anticipate that this is probably due to the surface-sensitivity of NEXAFS spectroscopy when acquired in TEY mode, which implies that only the surface of the catalyst particles is probed, and not the interior. This hypothesis will be discussed later in the paper.

Finally, Fig. 1C shows the DR UV–Vis-NIR spectra of the catalysts obtained in the presence of increasing amounts of TEAl, from Al/Ti = 0.65 to Al/Ti = 3.25; the corresponding second derivative curves are reported in Fig. S1, to better appreciate the position of the absorption bands mentioned here below. The spectral behaviour upon TEAl addition can be divided in two main steps. The initial addition of TEAl (up to 1.0 eq.) causes the decrease in intensity of the band at about 28000 cm^{-1}, which was assigned to a ligand-to-metal charge-transfer transition of the type $Cl(\pi) \rightarrow Ti(d_{t2g})$ involving Ti(IV) sites in a distorted octahedral coordination. Simultaneously, the band at about 39,000 cm^{-1} increases in intensity,

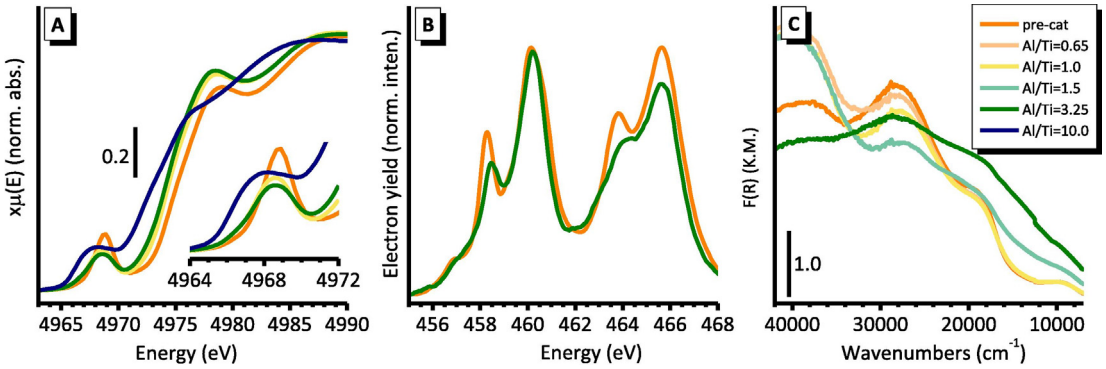

Fig. 1. Normalized Ti K-edge XANES (part A), normalized Ti L_3-edge NEXAFS spectra (part b) and DR UV–Vis-NIR (part C) of the SiO_2-supported precatalyst, and of the same sample after activation with TEAl in different amount (expressed in terms of Al/Ti ratio). The inset in part A shows a magnification of the pre-edge peak.

suggesting that a fraction of the 6-fold coordinated Ti(IV) sites are reduced to Ti(III). Indeed, the optical electronegativity rule of Jorgensen [27] predicts that the Cl(π) → Ti(d_{t2g}) charge-transfer transition should shift upward of at least 7000 cm^{-1} upon reduction of Ti(IV) to Ti(III). The presence of intense bands in the visible part of the spectrum prevents the observation of the much weaker d-d transitions that should characterize isolated Ti(III) species. When the precatalyst is activated with larger amounts of TEAl the spectral shape completely changes, with the appearance of two very intense bands at ca. 22,000 and 15500 cm^{-1}, the latter with a pronounced tail at lower energy. These bands are assigned to inter-site hopping transitions of the type $2(3d^1) \rightarrow 3d^0 + 3d^2$ involving two Ti (III) sites bridged by a common chlorine ligand, similar to what observed for the α-$TiCl_3$ polymorph [23,28–30].

The results discussed so far demonstrate that addition of small amounts of TEAl (below 1.0 eq.) to the silica-supported precatalyst leads to the reduction of a fraction of the Ti(IV) sites to isolated Ti (III) species, while larger amounts of TEAl not only complete the reduction of the Ti(IV) sites, but also cause the aggregation of Ti (III) species to clusters having electronic properties similar to those of the α-$TiCl_3$ polymorph, eventually over-reducing a fraction of the Ti species to Ti(II). The data at our disposal do not allow to define the *mechanism of formation* of these α-$TiCl_3$ clusters. Nevertheless, we are tempted to exclude that they are formed starting from previous Ti(IV) aggregates, since the data reported in Part 1 of this same story [8] exclude the proximity of Ti(IV) sites in the precatalyst, and moreover α-$TiCl_3$ clusters are formed only upon exciding a certain A/Ti ratio. It is more likely that there is a certain mobility after Ti(III) formation. The literature supports this second hypothesis. It has been reported that addition of a strong Lewis acid such as ethyl aluminum dichloride causes part of the Ti(III) in the solid phase to resolubilize, a phenomenon commonly referred to as leaching [31,32]. In particular, $Ti(OR)_{3-x}Cl_x$ complexes of the type proposed in Part 1 [8] are insoluble in hydrocarbons, but can be detached from the catalyst surface upon extended contact time with the Lewis acid. As far as the *location* of these different Ti(III) species on the catalyst particles is concerned, it is important to notice that the invariance of the Ti $L_{2,3}$-edge NEXAFS spectrum to TEAl addition suggests that the $TiCl_3$ clusters (both those originally present in the precatalyst and those induced by activation with TEAl) are mainly formed at the exterior of the catalyst particles. In fact, as demonstrated in our previous work [23], the experimental Ti $L_{2,3}$-edge NEXAFS spectra of $TiCl_3$ polymorphs are very similar to the spectrum of highly dispersed Ti(IV) chloride species. Hence, in the presence of $TiCl_3$ clusters at the exterior of the catalyst particles, the Ti $L_{2,3}$-edge NEXAFS spectrum collected in TEY mode will be invariably dominated by their signals, making virtually impossible to reveal the reduction of isolated Ti(IV) sites.

3.2. Local structure of the Ti sites

Fig. 2 shows the Fourier-Transformed k^2-weighted EXAFS function of the catalyst activated with increasing amounts of TEAl, in both Modulus (part A) and Imaginary (part B) parts. With respect to the spectrum of the precatalyst, addition of 1.0 and 3.25 eq. of TEAl leads to the decrease in intensity of the first peak (centred at ca. 1.35 Å, phase-uncorrected) and to the increase of the second one (centred at ca. 2.07 Å, phase-uncorrected). It is worth remembering that, according to the data analysis discussed in Part 1 of this work [8], these two peaks do not correspond to the contribution of two types of neighbours at two different distances from the Ti absorber, rather they are the result of the overlap of two/three types of chlorine ligands and/or one oxygen ligand, characterized by different bond distances. The observed changes indicate that addition of TEAl causes important modification of the local structure around the Ti sites.

The analysis of these data is complicated by the co-existence of more than two Ti phases, as suggested by the other techniques. Two of them were already present in the precatalyst, as discussed in part 1 of this story [8]: 1) $TiCl_3$ clusters resembling the β-$TiCl_3$ polymorph; 2) monomeric Ti(IV) sites with a very heterogeneous local structure, which are only partially converted to Ti(III) sites, in an amount which depends on the Al/Ti ratio. Additionally, two new phases are generated by activation: 3) isolated Ti(III) sites formed via the reduction of monomeric Ti(IV) sites; 4) $TiCl_3$ clusters similar to the α-$TiCl_3$ polymorph, whose formation is promoted by amounts of TEAl larger than 1.0 eq., which likely derive from mobilization and aggregation of $Ti(OR)_{3-x}Cl_x$ complexes, as discussed above. In these conditions, it is not possible to extract meaningful quantitative results from the EXAFS data analysis.

Finally, addition of 10 eq. of TEAl, which corresponds to an over-reduction of the Ti sites as determined by the XANES region, brings about a complete change in the EXAFS spectrum. The first peak basically disappears and the amplitude of the second one is damped. Moreover, at longer distances the signal due to the multiple scattering contributions of collinear Cl-Ti-Cl paths is totally disrupted. This spectrum is distinctly different with respect to that of β-$TiCl_3$. This confirms that over-reduction deeply involves the β-$TiCl_3$ clusters already present in the precatalyst, generating a highly disordered titanium chloride phase.

3.3. Accessibility of the surface sites and their involvement in ethylene polymerization

In the absence of structural details on the activated catalysts, we turned our attention to IR spectroscopy of adsorbed CO as a

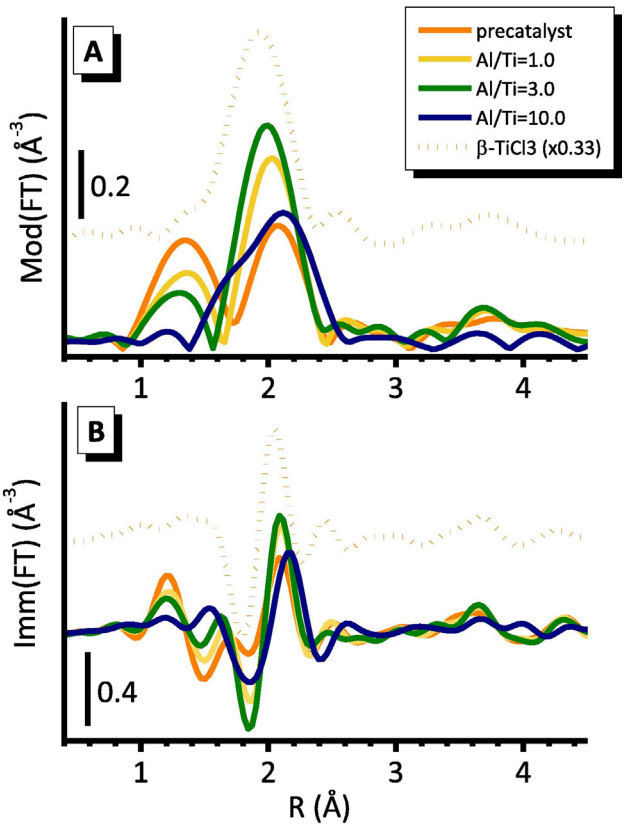

Fig. 2. K^2-weighted |FT| (part A) and Imm(FT) (part B) of the EXAFS function for the precatalyst, and of the same sample after activation with TEAl in different amount (expressed in terms of Al/Ti ratio). The spectrum of the β-$TiCl_3$ reference is also reported for comparison, vertically translated for clarity.

method to probe the accessible surface sites and, indirectly, to extract information on their coordination and insertion ability. At first, we monitored by IR spectroscopy the adsorption of CO at 100 K on a catalyst activated with 3.25 eq of TEAl. Fig. 3A shows the sequence of IR spectra, in the ν(CO) region, collected at 100 K upon decreasing the CO pressure (P_{CO}). At the maximum CO coverage, the spectrum is characterized by a broad band centred around 2155 cm^{-1}, a sharp band at 2137 cm^{-1} and a well-defined band at 2065 cm^{-1}. Upon decreasing P_{CO} the sharp band at 2137 cm^{-1}, which is ascribed to physisorbed CO [33], rapidly decreases in intensity, followed by that at 2155 cm^{-1}, which becomes more structured, clearly revealing two components at 2184 and 2157 cm^{-1}. These latter bands are reminiscent of those observed, with much higher intensities, in the spectrum of CO adsorbed at 100 K on the precatalyst and assigned to CO adsorbed on 4-fold and 5-fold coordinated Mg^{2+} cations [34–37], respectively. This indicates that in the presence of TEAl (and of its reaction by-products), most of the previously exposed Mg^{2+} cations are no more accessible.

The band at 2065 cm^{-1}, which is much more resistant to degassing, is attributed to CO adsorbed on reduced Ti(III) sites. Similar bands were previously observed for CO adsorbed on different types of ZN (pre)catalysts, specifically at: 2091 cm^{-1} for an industrial $MgCl_2$-based ZN precatalyst [38]; 2076 cm^{-1} for a model $MgCl_2$/$TiCl_4$ catalyst activated by TEAl [39]; at 2055 and 2049 cm^{-1} for $MgCl_2$-based ZN catalysts activated by TEAl, both containing a 1,3-diether as internal donor (ID) but prepared with different procedures [40]. For comparison, the ν(CO) stretching frequency for the $Cp_2Ti(C_5F_6)(CO)$ and $(C_5Me_5)_2TiCl(CO)$ complexes have been reported at 2060 cm^{-1} and 2000 cm^{-1}, respectively, while the IR spectrum of $Cp_2Ti(CO)_2$ shows two bands at 1964 and 1883 cm^{-1} [41–44]. In general terms, the position of the ν(CO) band is the result of a balance between the polarizing effect of the Ti ion and the π-back-donation ability due to the unpaired d electron. An increase in the effective charge at the Ti sites stabilizes and contracts the d orbitals, resulting in a less efficient overlap with the CO anti-bonding orbital for π back-donation, and hence in ν(CO) at higher values. Notably, the few data available in the literature for CO adsorbed on ZN catalysts allows us to observe a trend: the ν(CO) band is observed at higher frequency in the absence of IDs. This is in agreement with previous findings [45,46], according to which the presence of IDs nearby the alkylated Ti^{3+} sites should increase the Ti electron density, since the ionic nature of the system allows Ti species to electronically feel the surrounding environment in a remote fashion. The band at 2165 cm^{-1} observed in the present case follows the same trend, since no IDs are intentionally introduced in the formulation of our catalyst.

The observation of the band at 2065 cm^{-1} in Fig. 3A (not observed upon CO adsorption on the precatalyst) clearly demonstrates that a fraction of Ti(III) sites, originating from the activation with TEAl, are accessible by CO. At this point, we did a step further, trying to monitor the CO insertion ability of these accessible, probably alkylated, Ti(III) sites. It is well established that insertion of CO into the metal-alkyl bond follows CO coordination at the metal site, and usually is a slow process. For this reason, we performed a second IR experiment, monitoring CO adsorption at room temperature on the same catalyst (activated with 3.25 eq. of TEAl), as a function of time. The sequence of IR spectra collected during 1 h of reaction are reported in Fig. 3B for the ν(CO) region of coordinated CO and in Fig. 3C for the ν(C = O) region of inserted CO. Fig. 3B' and Fig. 3C' show the first (after 1 min) and last (after 1 h) spectra, after removal of the spectrum of gaseous CO and a slight smoothing procedure.

After 1 min from CO dosage (dark green), the IR spectrum shows the same bands at 2065 and 2137 cm^{-1} already detected in the experiment performed at 100 K, the latter band being visible only after removal of the roto-vibrational profile of gaseous CO. However, upon waiting in time, new bands appear and gradually grow in intensity at 2022, 1658 and 1548 cm^{-1}. The former band is ascribed to CO coordinated on a second type of Ti(III) sites, with a higher π back-donation ability than those responsible for the band at 2065 cm^{-1}, but less accessible. This ν(CO) value is even lower than that observed on ZN catalysts containing IDs [40] and suggests that this second family of alkylated Ti(III) sites are characterized by an even higher electron density. A possible hypothesis to explain this experimental observation is to take into account the possible presence of aluminum alkoxides nearby, which are among the potential by-products of reaction with TEAl and would act as unintentional electron donors. The two bands at 1658 and 1548 cm^{-1}, instead, are ascribed to ν(C=O) of Ti-acyl species, originated upon insertion of CO into the Ti-ethyl bond. According to the literature, acyl derivatives of titanocene complexes of the type $Cp_2Ti(X)R$ or CpTiR are characterized by ν(C=O) values that can range from 1620 to 1470 cm^{-1}, depending on the nature of the X and R groups, and on the extent of the η^2-coordination to the Ti sites: the larger the η^2-coordination, the lower ν(C=O) [41–44].

All in all, the spectra reported in Fig. 3 do suggest the existence of at least two types of Ti(III) sites with a different electron density accessible to CO: coordination of CO is immediate in one case, while it is kinetically slower in the other. Two types of Ti-acyl species are also formed upon insertion of CO into the Ti-alkyl bond, characterized by different extent of η^2-coordination with Ti. Whether the two types of Ti-acyl species are formed from the two types of Ti(III) sites which coordinate CO or only one, is difficult to say at this stage.

The same experiment discussed above was repeated after ethylene polymerization (Fig. S2). Briefly, the catalyst activated with

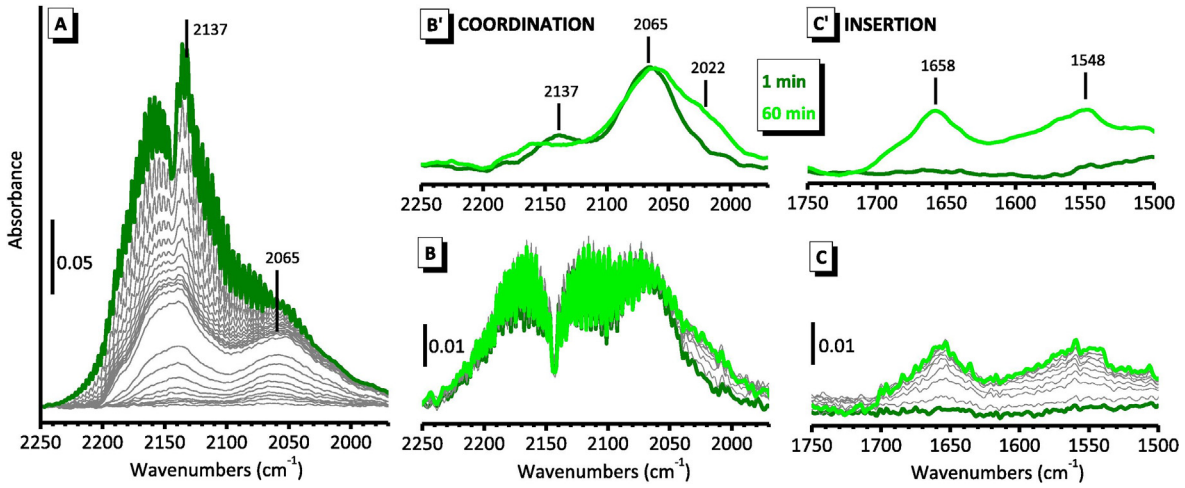

Fig. 3. Part A: FT-IR spectra (in the ν(CO) region) of CO adsorbed at 100 K on the catalyst activated with 3.25 eq. of TEAl as a function of the CO coverage Θ (from Θ_{max} in orange, to zero in dark grey). The spectra are shown after subtraction of the spectrum prior the dosage of CO. Part B: FT-IR spectra (in the ν(CO) region) of CO adsorbed at room temperature on the catalyst activated with 3.25 eq. of TEAl as a function of time (dark green: after 1 min; light green: after 1 h). The spectra are shown after subtraction of the spectrum prior the dosage of CO. Part C: the same as part B but in the ν(C=O) region of the Ti-acyl species. Parts B' and C': initial and final spectra reported in parts B and C after removal of the spectrum of gaseous CO and smoothing, to better observe the absorption bands. (For interpretation of the references to colour in this figure legend, the reader is referred to the web version of this article.)

3.25 eq. of TEAl was contacted with ethylene for 10 min. After that, ethylene gas was removed from the cell, and CO was admitted. The results indicate that the Ti(III) sites are almost no more accessible after ethylene polymerization, and consequently only a very minor amount of acyl species is observed. This is probably explainable in terms of formation, in these experimental conditions, of a thick layer of PE on the external surface of the catalyst particles preventing CO from reaching the active sites, as it will be demonstrated in the following.

3.4. The catalyst in action

3.4.1. Kinetics of ethylene polymerization

We evaluated the kinetics of ethylene polymerization under very mild conditions (similar to those adopted during the spectroscopic measurements) as a function of the Al/Ti ratio. Fig. 4 shows the reciprocal of the ethylene pressure as a function of time. It is evident that, irrespective of the amount of TEAl used for activation, the experimental data are fitted excellently by a straight line, which indicates second order kinetics. The activity increases upon increasing the Al/Ti ratio. These data are in agreement with some of the literature on ethylene homo-polymerization on supported Ti-based Ziegler catalysts, where reaction orders as high as 1.7–2.0 can be found, in contrast to what observed in the presence of other α-olefins, such as propene [47]. The problem regarding the dependence of ethylene polymerization rate on monomer concentration is still controversial [48], and several explanations have been proposed to account for this unusual behaviour. Most of them brings up a dynamic equilibrium between active Ti-alkyl species with (at least) one open coordination vacancy available for ethylene insertion, and inactive (or dormant) species with the Ti coordination sphere being saturated, hence not being available for ethylene coordination. For example, according to the "trigger" mechanism proposed by Ystenes [49], an ethylene molecule coordinated to an active site can be incorporated into the propagating chain only when a second ethylene molecule is coordinated, that is, only if the Ti-alkyl species has at least two open coordination vacancies. For Matsko et al. [48] the coordination sphere in inactive Ti-alkyl species is saturated by excess of Al-alkyl but may become active via interaction with ethylene. According to Kissin et al. [50–52] an inactive Ti-CH_2CH_3 species is rapidly formed from the active

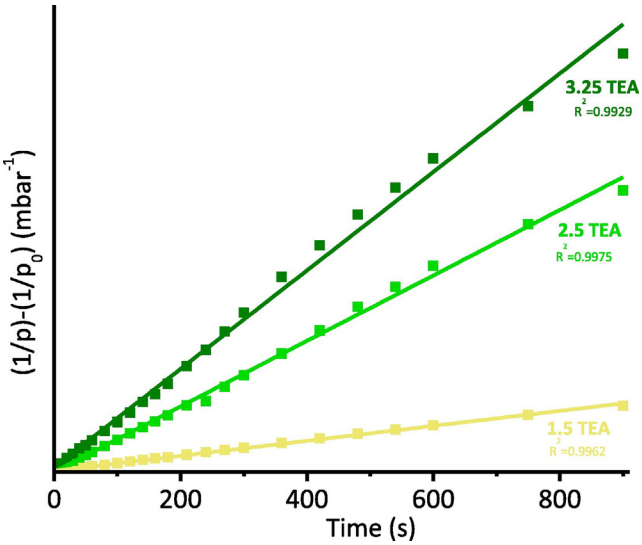

Fig. 4. Kinetics of ethylene polymerization for catalysts activated with increasing amounts of TEAl. The experimental data are reported as squares, while the lines are the best linear fits (with indicated R^2 values).

one in ethylene deficiency via a strong β-agostic interaction with the hydrogen atom of the methyl group.

At present we have no experimental evidences for describing the structure of the active and dormant Ti sites. However, our observation by IR spectroscopy of two types of Ti-acyl species in the presence of CO, of which one is characterized by a strong η^2-coordination with Ti, suggests that also C–H agostic interactions might play a role in the equilibrium between active and dormant sites. We speculate that the Ti-alkyl sites forming η^2-coordinated acyl species in the presence of CO are also those prone to becoming inactive during ethylene polymerization through C–H agostic interactions.

3.4.2. Fragmentation behaviour during ethylene polymerization

The morphological evolution of the ZN catalyst during slurry-phase ethylene polymerization was investigated both in the presence of TEAl (3.13 eq.) and TiBA (3.25 eq.). At 1 bar ethylene pres-

sure, the two samples produced similar PE yields after 1 min of polymerization. Both the TEAl- and TiBA-activated catalyst particles also display comparable morphologies: a pronounced build-up of PE at the particle surface can be observed (Fig. 5) and is attributed to fast catalyst kinetics in the most accessible regions of the catalyst particles, as previously reported in the literature [53]. The accumulation of polymer, in combination with the onset of polymerization further into the particle interiors, results in the formation of radial fractures (early stages of the sectioning fragmentation mechanism), as clearly visible in the cross-section of the TiBA-activated particle. Irrespective of the co-catalyst type, an immediate formation of polyethylene occurs at the particle surface, thus confirming the presence of active Ti(III) sites.

3.4.3. Fragmentation of the catalyst particles facilitates the detection of the active sites by Ti $L_{2,3}$-edge NEXAFS spectroscopy

Finally, the behaviour of the catalyst in the presence of ethylene was investigated by Ti $L_{2,3}$-edge NEXAFS spectroscopy in TEY. Fig. 6 shows the spectrum of the catalyst activated with 3.25 eq. of TEAl (the same discussed in Fig. 1) and a sequence of spectra acquired after contacting the catalyst with small pulses of ethylene. The spectra change significantly immediately after the first ethylene pulse and even more so in the next steps to a degree that the final spectrum is completely different from the initial one. In particular, the final spectrum is half less intense than the initial one, and in the L_3 region shows new peaks at 456.5, 458.2 and 459.5 eV, which are very similar to those observed by some of us in the Ti L_3-edge NEXAFS of a model $MgCl_2$-supported ZN catalyst after activation by TEAl, and assigned to monomeric and alkylated Ti(III) species [23].

While the decrease in intensity of the overall spectrum can be easily explained by the formation of an insulating PE layer, which decreases the probability to collect the electrons escaping from the sample, the change in the spectral shape is completely unexpected. Indeed, we should not expect relevant changes in the electronic features of the active sites upon ethylene insertion into the Ti (III)-alkyl bond, since a polymeric chain is not dissimilar from an alkyl group. When a similar experiment was performed on the model $MgCl_2$-supported ZN catalyst mentioned above, ethylene polymerization simply led to the disappearance of the spectral components that were attributed to the active sites [23]. This was explained with the hypothesis that, in the initial stages of the reaction, the formed PE selectively masks the active sites, where it is formed.

The sequence of spectra reported in Fig. 6 suggests that during ethylene polymerization, new Ti(III) sites, previously escaping detection, gradually emerge at the surface, and are thus detected by TEY-NEXAFS. This is exactly what we expect to occur during cat-

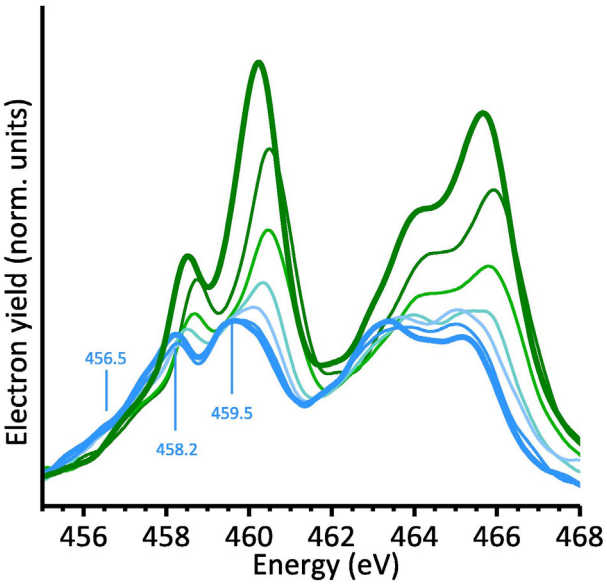

Fig. 6. Ti $L_{2,3}$-edge NEXAFS spectrum of the catalyst activated with 3.25 eq. of TEAl (green bold) and evolution of the spectra in the presence of small ethylene pulses (from green to blue). The whole sequence of spectra was collected within a few minutes. (For interpretation of the references to colour in this figure legend, the reader is referred to the web version of this article.)

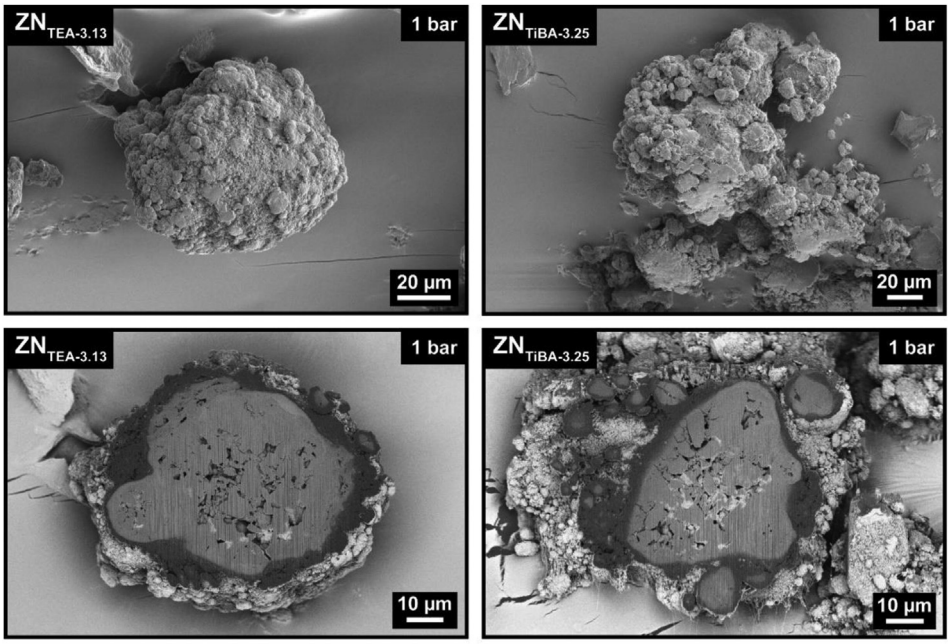

Fig. 5. Scanning electron microscopy (SEM) images of the external and internal morphology of two catalyst particles that were pre-polymerized for 1 min at 1 bar ethylene pressure in the presence of triethylaluminium (TEAl) and tri-isobutylaluminum (TiBA) in slurry-phase (room temperature; heptane; yields: 3.13 eq. TEA: 3.17 g_{PE}/g_{cat}, 3.25 eq. TiBA: 3.53 g_{PE}/g_{cat}).

alyst particle fragmentation. We conclude that the experimental procedure adopted here during the NEXAFS experiment (i.e., small ethylene pulses under inert flow), which was necessary for performing the measurements in total electron yield, also allowed to reduce the polymerization rate in the early reaction stages, thus avoiding the formation of a PE layer at the exterior of the catalyst particles. This allowed the entrance of ethylene and the growth of PE inside the particles, with a consequent stress build-up ultimately favouring (serendipitously) the fragmentation of the catalyst.

4. Conclusions

We have investigated in this work the properties of a highly active silica-supported ZN catalyst industrially employed for PE production at different length scales. Initially we focused our attention on the effects of the Al-alkyl activator (type and concentration) on the structure and accessibility of the Ti sites at a molecular level. By combining several highly sensitive spectroscopic methods we proved the co-existence of numerous Ti phases, differing both in terms of oxidation (Ti(IV), Ti(III) and even Ti(II)) and aggregation (isolated or clusters) state, whose relative amount is a function of the Al/Ti molar ratio. The accessible Ti(III) sites in the activated catalyst were probed by CO, which is a molecule that is not only able to coordinate to the Ti sites but also to insert into the Ti-alkyl bond, mimicking the behaviour of an olefin monomer. Two types of Ti(III) sites were distinguished: one with a higher effective charge (i.e. lower electron density), which is immediately accessible, and a second with a lower effective charge (i.e. higher electron density) and slower CO coordination kinetics. Also, two type of Ti-acyl species were formed upon insertion of CO into the Ti-alkyl bond, differing in the extent of the η^2-coordination to Ti.

In a second step, we have investigated the behaviour of the catalyst during ethylene polymerization under mild conditions. Second order kinetics were found for ethylene polymerization in the gas-phase at any Al/Ti ratio, in agreement with literature. This suggests an equilibrium between active and dormant Ti sites, likely tuned by C–H agostic interactions. During slurry-phase ethylene polymerization at 1 bar, PE immediately forms at the surface of the catalyst particles. The observation of a few radial fractures indicates a more dominant contribution from the sectioning fragmentation mechanism during the early stages of the reaction.

Considering the whole set of spectroscopic data discussed above, hypotheses on the spatial distribution of the different Ti phases in the catalyst particles can be made. The formation of $TiCl_3$ clusters, both during the catalyst synthesis and during the catalyst activation by trialkyl aluminum, is likely due to a mobilization and further aggregation of reduced $Ti(OR)_{3-x}Cl_x$ species in the presence of strong Lewis acids and is favoured at the exterior of the catalyst particles. When $TiCl_3$ clusters are present, their electronic features invariably dominate both the Ti $L_{2,3}$-edge NEXAFS and DR UV–Vis spectra, hampering the detection of isolated Ti(III) species. However, the fact that isolated Ti(III) species are present also at the exterior of the activated catalyst particle is demonstrated by IR spectroscopy, which detects a family of alkylated Ti(III) sites able to coordinate CO immediately. The corresponding ν(CO) band indicates that these Ti(III) species have an electron density compatible with the absence of electron donors nearby. In contrast to this, only monomeric Ti species are formed inside the catalyst particles, both during the precatalyst synthesis (in the form of Ti(IV)) and during catalyst activation (in the form of alkylated Ti(III)). These species coordinate CO at longer times due to diffusion limitations, and become visible by Ti $L_{2,3}$-edge NEXAFS only after pronounced catalyst particle fragmentation, which is achieved by working under very mild pre-polymerization conditions. The corresponding ν(CO) suggests the presence of electron donors in the close proximity of these Ti(III) sites, which might be the aluminum alkoxide species unintentionally formed as by-products of the reaction with TEAl.

Data availability

Data will be made available on request.

Declaration of Competing Interest

The authors declare that they have no known competing financial interests or personal relationships that could have appeared to influence the work reported in this paper.

Acknowledgments

This work forms part of the research program of DPI, project #813, and has been partially performed in the framework of the Nanoscience Foundry and Fine Analysis (NFFA-MUR Italy Progetti Internazionali) facility. The authors acknowledge support from Project CH4.0 under MUR (Italian Ministry for the University) program “Dipartimenti di Eccellenza 2023-2027” (CUP: D13C22003520001).

Appendix A. Supplementary data

Supplementary data to this article can be found online at https://doi.org/10.1016/j.jcat.2023.04.015.

References

[1] T.E. Nowlin, R.I. Mink, F.Y. Lo, T. Kumar, Ziegler-natta catalysts on silica for ethylene polymerization, J. Polym. Sci. A Polym. Chem. 29 (1991) 1167–1173.
[2] T.J. Pullukat, R.E. Hoff, Silica-based Ziegler-Natta catalysts: a patent review, Catal. Rev. Sci. Eng. 41 (1999) 389–428.
[3] M.J. Werny, R. Valadian, L.M. Lohse, A.L. Robisch, S. Zanoni, C. Hendriksen, B.M. Weckhuysen, F. Meirer, X-ray nanotomography uncovers morphological heterogeneity in a polymerization catalyst at multiple reaction stages, Chem. Catal. 1 (2021) 1413–1426.
[4] M. Ahsan Bashir, T.F.L. McKenna, Reaction engineering of polyolefins: the role of catalyst supports in ethylene polymerization on metallocene catalysts, in: Advances in Polymer Science, Springer, New York LLC, 2018, pp. 19–63.
[5] T.J. Pullukat, R.E. Hoff, Polymerization Catalyst and Method, US4374753, 1983.
[6] M. Shida, T.J. Pullukat, R.E. Hoff, Polymerization Catalyst, US4263171, 1981.
[7] R.E. Hoff, Polymerization Catalyst and Method, US4402861, 1983.
[8] Zarupski J., Piovano A., Signorile M., Amodio A., Olivi L., Hendriksen C., Friederichs N. H., Groppo E., Silica-magnesium-titanium Ziegler-Natta catalysts. Part 1: structure of the pre-catalyst at a molecular level, J. Catal. Submitted.
[9] G. Takasao, T. Wada, A. Thakur, P. Chammingkwan, M. Terano, T. Taniike, Machine learning-aided structure determination for TiCl4-capped MgCl2 nanoplate of heterogeneous Ziegler-Natta catalyst, ACS Catal. 9 (2019) 2599–2609.
[10] K. Seenivasan, A. Sommazzi, F. Bonino, S. Bordiga, E. Groppo, Spectroscopic investigation of heterogeneous Ziegler-Natta catalysts: Ti and Mg chloride tetrahydrofuranates, their interaction compound, and the role of the activator, Chem. Eur. J. 17 (2011) 8648–8656.
[11] E. Groppo, E. Gallo, K. Seenivasan, K.A. Lomachenko, A. Sommazzi, S. Bordiga, P. Glatzel, R. Van Silfhout, A. Kachatkou, W. Bras, C. Lamberti, XAS and XES techniques shed light on the dark side of Ziegler-Natta catalysts: active-site generation, ChemCatChem 7 (2015) 1432–1437.
[12] K. Seenivasan, E. Gallo, A. Piovano, J.G. Vitillo, A. Sommazzi, S. Bordiga, C. Lamberti, P. Glatzel, E. Groppo, Silica-supported Ti chloride tetrahydrofuranates, precursors of Ziegler-Natta catalysts, Dalton Transactions 42 (2013).
[13] E. Groppo, K. Seenivasan, E. Gallo, A. Sommazzi, C. Lamberti, S. Bordiga, Activation and in situ ethylene polymerization on silica-supported Ziegler-Natta catalysts, ACS Catal. 5 (2015) 5586–5595.
[14] I. Tritto, M. Carmela Sacchi, P. Locatelli, On the insertion reaction of carbon oxides into metal-carbon bonds of Ziegler-Natta catalysts, Macromol. Chem. Rapid Comm. 4 (1983) 623–627.
[15] Y. Doi, M. Murata, K. Yano, T. Keii, Gas-phase polymerization of propene with the supported ziegler catalyst: $TiCl_4/MgCl_2/C_6H_5COOC_2H_5/Al(C_2H_5)_3$, Ind. Eng. Chem. Res. 21 (1982) 580–585.

[16] A. Thakur, T. Wada, P. Chammingkwan, M. Terano, T. Taniike, Development of large-scale stopped-flow technique and its application in elucidation of initial Ziegler-Natta olefin polymerization kinetics, Polymers 11 (2019) 1012–1034.
[17] T. Taniike, S. Sano, M. Ikeya, V.Q. Thang, M. Terano, Development of a large-scale stopped-flow system for heterogeneous olefin polymerization kinetics, Macromol. React. Eng. 6 (2012) 275–279.
[18] V. Busico, M. Guardasole, A. Margonelli, A.L. Segre, Insertion of carbon monoxide into Zr-polymeryl bonds: "Snapshots" of a running catalyst, J. Am. Chem. Soc. 122 (2000) 5226–5227.
[19] Z.-Q. Fan, L.-X. Feng, S.-L. Yang, Distribution of active centers on $TiCl_4/MgCl_2$ catalyst for olefin polymerization, J. Polym. Sci. A 34 (1996) 3329–3335.
[20] G.D. Bukatov, V.S. Goncharov, V.A. Zakharov, Interaction of 14CO with Ziegler-type heterogeneous catalysts and effect of interaction products on the determination of the amount of active centers, Die Makromolekulare Chemie 187 (1986) 1041–1051.
[21] T. Shiono, M. Ohgizawa, K. Soga, Reaction between carbon monoxide and a Ti-polyethylene bond with a $MgCl_2$-supported $TiCl_4$ catalyst system, Die Makromolekulare Chemie 194 (1993) 2075–2085.
[22] C. Castán-Guerrero, D. Krizmancic, V. Bonanni, R. Edla, A. Deluisa, F. Salvador, G. Rossi, G. Panaccione, P. Torelli, A reaction cell for ambient pressure soft x-ray absorption spectroscopy, Rev. Sci. Inst. 89 (2018).
[23] A. Piovano, M. Signorile, L. Braglia, P. Torelli, A. Martini, T. Wada, G. Takasao, T. Taniike, E. Groppo, Electronic properties of Ti Sites in Ziegler-Natta catalysts, ACS Catal. 11 (2021) 9949–9961.
[24] D.A.M. De Winter, F. Meirer, B.M. Weckhuysen, FIB-SEM tomography probes the mesoscale pore space of an individual catalytic cracking particle, ACS Catal. 6 (2016) 3158–3167.
[25] M.J. Werny, J. Zarupski, I.C. ten Have, A. Piovano, C. Hendriksen, N.H. Friederichs, F. Meirer, E. Groppo, B.M. Weckhuysen, Correlating the morphological evolution of individual catalyst particles to the kinetic behavior of metallocene-based ethylene polymerization catalysts, JACS Au. 1 (2021) 1996–2008.
[26] P. Perlepe, I. Oyarzabal, L. Voigt, M. Kubus, D.N. Woodruff, S.E. Reyes-Lillo, M.L. Aubrey, P. Négrier, M. Rouzières, F. Wilhelm, A. Rogalev, J.B. Neaton, J.R. Long, C. Mathonière, B. Vignolle, K.S. Pedersen, R. Clérac, From an antiferromagnetic insulator to a strongly correlated metal in square-lattice $MCl_2(pyrazine)_2$ coordination solids, Nat. Comm. 13 (2022) 1–7.
[27] C.K. Jorgensen, Absorption Spectra and Chemical Bonding in Complexes, 1st ed., Pergamon Press, 1962.
[28] R.J.H. Clark, Diffuse-reflectance spectra of some anhydrous transition-metal halides, J. Am. Chem. Soc. 253 (1964) 417–425.
[29] I. Pollini, Electronic transitions in α- and β-titanium trichloride, Solid State Commun. 47 (1983) 403–408.
[30] C.H. Maule, J.N. Tothill, P. Strange, J.A. Wilson, An optical investigation into the 3d1 and 3d2 transition-metal halides and oxyhalides, compounds near to delocalisation, J. Phys. C 21 (1988) 2153.
[31] S. Cucinella, A. Mazzei, W. Marconi, C. Busetto, Reactions between $AlRCl_2$ and $Ti(OR)_4$ and activity in diolefin polymerization, J. Macromol. Sci. Chem. 4 (1970) 1549–1561.
[32] A. Klaue, M. Kruck, N. Friederichs, F. Bertola, H. Wu, M. Morbidelli, Insight into the synthesis process of an industrial Ziegler-Natta catalyst, Ind. Eng. Chem. Res. 58 (2019) 886–896.
[33] A. Zecchina, C. Otero Arean, Diatomic molecular probes for mid-IR studies of zeolites, Chem Soc Rev. 25 (1996) 187–197.
[34] A. Piovano, M. D'Amore, K.S. Thushara, E. Groppo, Spectroscopic evidences for $TiCl_4$/donor complexes on the surface of $MgCl_2$-supported Ziegler-Natta catalysts, J. Phys. Chem. C 122 (2018) 5615–5626.
[35] M. D'Amore, K.S. Thushara, A. Piovano, M. Causà, S. Bordiga, E. Groppo, Surface investigation and morphological analysis of structurally disordered $MgCl_2$ and $MgCl_2/TiCl_4$ Ziegler-Natta catalysts, ACS Catal. 6 (2016) 5786–5796.
[36] K.S. Thushara, M. D'Amore, A. Piovano, S. Bordiga, E. Groppo, The influence of alcohols in driving the morphology of magnesium chloride nanocrystals, ChemCatChem. 9 (2017) 1782–1787.
[37] A. Piovano, M. D'Amore, T. Wada, P. Cleto Bruzzese, G. Takasao, A. Thakur, P. Chammingkwan, M. Terano, B. Civalleri, S. Bordiga, T. Taniike, E. Groppo, Revisiting the identity of δ-$MgCl_2$: Part II. Morphology and exposed surfaces studied by vibrational spectroscopies and DFT calculation, J. Catal. 387 (2020) 1–11.
[38] P. Pletcher, A. Welle, A. Vantomme, B.M. Weckhuysen, Quality control for Ziegler-Natta catalysis via spectroscopic fingerprinting, J. Catal. 363 (2018) 128–135.
[39] A. Piovano, J. Zarupski, E. Groppo, Disclosing the interaction between carbon monoxide and alkylated Ti^{3+}species: a direct insight into Ziegler-Natta catalysis, J. Phys. Chem. Lett. 11 (2020) 5632–5637.
[40] M. Milanesi, A. Piovano, T. Wada, J. Zarupski, P. Chammingkwan, T. Taniike, E. Groppo, Influence of the synthetic procedure on the properties of three Ziegler-Natta catalysts with the same 1,3-diether internal donor, Catal. Today. 418 (2023).
[41] E. Klei, J.H. Teuben, Reaction of an alkenyltitanocene, J. Organomet. Chem. 222 (1981) 79–88.
[42] F. Calderazzo, Synthetic and mechanistic aspects of inorganic insertion reactions. Insertion of carbon monoxide, Angew. Chem. Int. Ed. 16 (1977) 299–311.
[43] J.G. Murray, A metal carbonyl compound of titanium, J. Am. Chem. Soc. 81 (1959) 752–753.
[44] G. Fachinetti, C. Floriani, Insertion of carbon monoxide into titanium—carbon bonds, J. Organomet. Chem. 71 (1974) C5–C7.
[45] X. Zhao, Y. Zhang, Y. Song, G. Wei, XPS study of interaction of titanium species with different internal electron donors on ZN catalysts, Surface Review and Letters 14 (2012) 951–955.
[46] T. Taniike, M. Terano, Coadsorption model for first-principle description of roles of donors in heterogeneous Ziegler-Natta propylene polymerization, J. Catal. 293 (2012) 39–50.
[47] R. Hoff, R.T. Mathers, Transition Metal Polymerization Catalysts, 1st ed., John Wiley & Sons, New Jersey, 2018.
[48] M.A. Matsko, V.A. Zakharov, M.I. Nikolaeva, T.B. Mikenas, Kinetics of ethylene polymerization over titanium-magnesium catalysts: the reasons for the observed second order of polymerization rate with respect to ethylene, Polyolefins Journal. 2 (2015) 27–38.
[49] M. Ystenes, The trigger mechanism for polymerization of alpha-olefins with Ziegler-Natta catalysts: a new model based on interaction of two monomers at the transition state and monomer activation of the catalytic centers, J. Catal. 129 (1991) 383–401.
[50] Y.V. Kissin, Peculiarities of ethylene polymerization reactions with heterogeneous Ziegler-Natta catalysts: kinetic analysis, Macromolecular Theory and Simulation. 11 (2002) 67–76.
[51] Y.V. Kissin, R.I. Mink, T.E. Nowlin, Ethylene polymerization reactions with ziegler-natta catalysts. I. Ethylene polymerization kinetics and kinetic mechanism, J. Polym. Sci. A Polym. Chem. 37 (1999) 4255–4272.
[52] Y.V. Kissin, R.I. Mink, T.E. Nowlin, A.J. Brandolini, Kinetics and mechanism of ethylene homopolymerization and copolymerization reactions with heterogeneous Ti-based Ziegler-Natta catalysts, Top Catal. 7 (1999) 69–88.
[53] M.J. Werny, D. Müller, C. Hendriksen, R. Chan, N.H. Friederichs, C. Fella, F. Meirer, B.M. Weckhuysen, Elucidating the sectioning fragmentation mechanism in silica-supported olefin polymerization catalysts with laboratory-based X-ray and electron microscopy, ChemCatChem 14 (2022) e202200067.